Stabilities in plane Poiseuille flow of Herschel-Bulkley fluid

R. Liu, Z. Ding, K.X. Hu

PII: S0377-0257(17)30124-6
DOI: 10.1016/j.jnnfm.2017.11.007
Reference: JNNFM 3950

To appear in: *Journal of Non-Newtonian Fluid Mechanics*

Received date: 18 March 2017
Revised date: 15 November 2017
Accepted date: 17 November 2017

Please cite this article as: R. Liu, Z. Ding, K.X. Hu, Stabilities in plane Poiseuille flow of Herschel-Bulkley fluid, *Journal of Non-Newtonian Fluid Mechanics* (2017), doi: 10.1016/j.jnnfm.2017.11.007

Highlights

- The Herschel-Bulkley model is used to describe the rheological behavior of a fluid with yield-stress and shear thinning
- The Herschel-Bulkley model is used to describe the rheological behavior of a fluid with yield-stress and shear thinning
- The shear thinning plays an important role in determining the stability and transient growth of the flow

Stabilities in plane Poiseuille flow of Herschel-Bulkley fluid

R. Liu[a,*], Z. Ding[b], K. X. Hu[c]

[a]*School of Mechanical and Electrical Engineering, Gui Lin University of Electronic Technology, Gui Lin 541004, China*
[b]*School of Mathematics, University of Bristol, Bristol BS8 1TW, United Kingdom*
[c]*School of Mechanical Engineering and Mechanics, Ningbo University, Ningbo 315211, China*

Abstract

Linear stability in plane Poiseuille flow of a yield-stress shear-thinning fluid is considered. The rheological behavior of the fluid is described by the Herschel-Bulkley model. The effect of shear-thinning on the stability is investigated using the energy method and the nonmodal stability theory. The result of the energy method shows that with the increase of shear thinning, the critical energy Reynolds number decreases for both the streamwise and spanwise disturbances. For the nonmodal stability, we focus on the response to initial conditions by examining the energy growth function $G(t)$. For a Herschel-Bulkley fluid, it is found that there can be a rather large transient growth even though the linear operator of the plan Poiseuille flow has no unstable eigenvalue. The results show that the shear thinning plays an important role in determining the energy growth rate and the structure of the disturbance with optimal transient growth.

Keywords: Herschel-Bulkley fluid; Plan Poiseuille flow; nonmodal stability

1. Introduction

Shear flows of viscoplastic fluids occur in many industrial processes, for example in oil wells, especially during drilling and cementing operations, and also

*Corresponding author
Email addresses: rongliu@guet.edu.cn (R. Liu), zding001@e.ntu.edu.sg (Z. Ding), hukaixin@nbu.edu.cn (K. X. Hu)

in the food processing and in mining industries [1]. Understanding the mechanisms of stability is of crucial importance for controlling the transition from laminar flow towards turbulence in many flow applications.

The fluid behavior of a viscoplastic material is characterized by the existence of a yield stress (τ_0) below which the material exhibits solid-like behavior and beyond which it exhibits liquid-like behavior. Most natural and industrial materials (glues, inks, pastes, slurries, paints, emulsions, foodstuffs, blood and drilling muds, etc.) obtained by suspending a large number of particles interacting via colloidal forces or direct contact in water fall into this category exhibiting a yield stress [2]. This yield stress is in fact the strength necessary to break the continuous network of interactions between particles throughout the sample. One of the most important characteristics of macromolecular fluids is the non-Newtonian viscosity, i.e., the fact that the viscosity μ changes with the shear rate $\dot{\gamma}$ [3]. A shear-thinning (shear-thickening) fluid, also called a pseudoplastic (dilatant) fluid, is a non-Newtonian fluid where the shear viscosity decreases (increases) with applied shear stress. Shear-thinning fluids are usually solutions of large, polymeric molecules in a solvent with smaller molecules. Most macromolecular fluids are shear-thinning, and shear-thickening fluids are rarely encountered [4].

The Bingham model has been widely used to describe the rheological behavior of a viscoplastic fluid [5]. One of the most important features of viscoplastic fluid flows, i.e. the presence of an unyielded zone and yield surface, has been rendered by this simple model. However, it has been found that some non-Newtonian fluids, such as yielded mud, may experience shear thinning at low shear stress level [6]. This is probably because the destruction of the internal structure responsible for the yield behaviour is a gradual process, during which the resistance to deformation becomes weaker, and is not completed until a high shear stress level is reached. It seems that more complex models, such as the Herschel-Bulkley model, are more appropriate in depicting this particular behavior. The constitutive laws for the Herschel-Bulkley model are formulated

by as

$$\begin{cases} \boldsymbol{\tau} = (\frac{\tau_0}{\dot{\gamma}} + K\dot{\gamma}^{n-1})\dot{\boldsymbol{\gamma}} \Leftrightarrow \tau \geq \tau_0, \\ \dot{\gamma} = 0 \Leftrightarrow \tau < \tau_0, \end{cases} \tag{1}$$

where μ is the effective viscosity, $\dot{\boldsymbol{\gamma}}$ is the rate of strain, $\boldsymbol{\tau}$ is the stress tensor, $\dot{\gamma}$ and τ are the second invariants of the rate-of-strain and deviatoric stress tensors, n is the power-law index representing the degree of shear thinning, K is the consistency factor, respectively. The most important features of viscoplastic fluid flows, i.e. yield stress and shear-thinning behavior of the effective viscosity are contained by the Herschel-Bulkley model, which is valid within a relatively wide shear rate range [7, 8].

Stability and transition to turbulence in shear flows have been studied extensively over the years. Traditionally, a first step in investigating transition is the normal mode analysis. For this approach, it is assumed that each mode has an exponential time dependence, thus the base flow is considered to be unstable if an eigenvalue is found in the unstable complex half-plane. The results of linear stability showed that for Newtonian fluids Poiseuille flow is linearly stable if the Reynolds number Re is less than the critical $Re_c \approx 5772$ [9] and that Couette flow is linearly stable for all Reynolds numbers [10]. However, experiments showed that Poiseuille and Couette flows may become unstable at Reynolds numbers as low as $Re \approx 1000$ [11] and ≈ 360 [12], respectively. Moreover, experiments showed that the route to turbulence is highly dependent on the initial conditions and on the continuous forcing that background noise can provide. The discrepancies between linear stability analysis and experiments have given rise to emergences of novel ways to investigate the mechanisms of transition.

Waleffe [14] proposed a new theory named the self-sustaining process (SSP) which arose out of efforts to understand how turbulence is maintained rather than initiated in subcritical condition. The self-sustaining process consists of three distinct phases. First, weak streamwise rolls redistribute the streamwise momentum to create streak structures with large spanwise fluctuations in the streamwise velocity. The spanwise inflections then lead to a wake-like instability

in which a three-dimensional disturbance of the form $e^{i\alpha x}\boldsymbol{u}(y,z)$ develops. The primary nonlinear effect resulting from the development of the instability is to reenergize the original streamwise rolls, leading to a time cycling of self-sustaining process.

Until now, no full theory of transition in shear flows exists. Nevertheless significant progress has been achieved due to the emergence of the nonmodal stability theory. The main point of departure of the nonmodal theory from the traditional eigenvalue analysis is the fact that even if all of the eigenvalues of a linear system are distinct and lie well inside the stable half plane, inputs to that system may be amplified by substantially large factors if the linear operator is non-normal [13].

Trefethen *et al.* [15] addressed the general concept of nonmodal stability and studied the response to external excitations and initial conditions for plane Couette and Poiseuille flows. Reddy and Henningson [16] computed the optimally amplified disturbances in channel flows using a singular value analysis. The results showed that initial states with largest transient energy growth in subcritical flows lead to flow structures that resemble streamwise vortices and streaks due to the "lift-up" mechanism [17, 18]. This mechanism works by efficiently extracting momentum from the mean flow and transferring it to the perturbation [19]. The transient growth of disturbance due to the nonmodal effect is responsible for the formation of streak in the first phase of SSP.

In recently years, the stabilities in channel or pipe flows of a yield stress fluid have given rise to special scientific interest. The most relevant works to the present paper are the studies on the modal [20] and nonmodal stabilities [21] of plane Poiseuille flow of a Bingham fluid. Frigaard *et al.* [20] studied the linear stability of two-dimensional disturbances in plane Poiseuille flow of a Bingham fluid. Unfortunately, the results are incomplete because even symmetry for the eigenfunction of the vertical velocity was imposed. Nouar and Frigaard [22] performed a nonlinear stability analysis based on the energy method. The results showed that the critical energy Reynolds number, Re, increases with Bingham number, B, at least as fast as $Re \sim B^{1/2}$ as $B \to \infty$. For non-Newtonian flu-

ids, three-dimensional disturbance should be considered for stability problems because Squire's theorem is not valid. Frigaard and Nouar [23] investigated the problem of eigenvalue bounds for three dimensional disturbances in plane Bingham-Poiseuille flow. It has been shown that three-dimensional linear stability can be achieved for a Reynolds number bound of form $Re = O(B^{3/4})$ as $B \to \infty$. Recently, Nouar *et al.* [24] investigated the stability of plane Bingham-Poiseuille flow in the framework of the nonmodal theory. The results showed that the optimal disturbance consists of almost streamwise vortices as $B \ll 1$, whereas the optimal disturbance becomes oblique for large B. The above works are limited to the plane shear flows. Esmael and Nouar [25], Liu and Liu [26] studied the non-modal stability of Hagen-Poiseuille flow of a yield stress fluid.

Although shear-thinning fluids are commonly used in industrial process, there is surprisingly little published work that focuses on transient behavior of these flows. Chikkadi *et al.* [27] have studied the transient growth of the plane Poiseuille flow of a Carreau fluid. Rather unexpectedly, the authors found that the transient growth is only slightly influenced by the shear-thinning effect. However, it should be noted that the results are only valid for neglecting the viscosity perturbations. Nouar *et al.* [28] have revisited the stability of shear-thinning fluids. The results showed that shear thinning appears to be destabilizing when Re is based on the average effective viscosity. Liu and Liu [29, 30] studied the shear-thinning effect on the stability of plane Couette flow and Hagen-Poiseuille flow. More recently, Bentrad *et al.* [31] have taken into account the shear thinning in Hagen-Poiseuille flow of a yield-stress fluid and studied the modal and nonmodal stability of the problem.

In the present paper, we consider the problem of the stability in plane Poiseuille flow of a yield stress shear-thinning fluid. Being different from the work by Nouar *et al.* [24], we used the Herschel-Bulkley model instead of the Bingham model to describe the constituent relation of the yield-stress fluid. For the Herschel-Bulkley model, the position of the yield surface is determined by both B and the power-law index n. In the present study, we focus on the influence of shear-thinning effect on the stability of the problem.

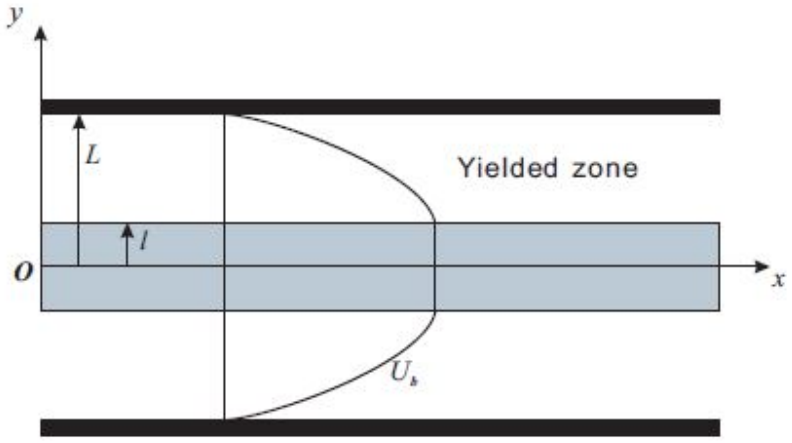

Figure 1: Sketch of the geometry of plane Poiseuille flow of a Herschel-Bulkley fluid.

The present paper is organized as follows. In Sec.2, the mathematical formulation of the physical model is presented. In Sec.3, the numerical method is presented. In Sec.4, we present the results and discussions. In Sec.5, we summarize the results and present the conclusions.

2. Mathematical formulation

A plane Poiseuille flow of an incompressible Herschel-Bulkley fluid with a yield stress τ_0 and a plastic viscosity μ is considered. The flow is driven by a constant pressure gradient in the streamwise direction. As shown in Fig.1, L is the half width of the chanel, l is the half width of the unyielded zone, $d = L - l$ is the width of the yielded zone, and U_0 is the maximum velocity of the base flow. To assess the effect of yield stress on the stability of the channel flows, it is important to employ an appropriate length scale. Because the flow is confined in the yielded flow region, it is appropriate to use d as the length scale instead of L.

We used d, d/U_0, U_0 and ρU_0^2 as the scales of length, time, velocity and

pressure. The Navier-Stokes equations are expressed in dimensionless form as:

$$\boldsymbol{\nabla} \cdot \boldsymbol{u} = 0 \tag{2}$$

$$\frac{\partial \boldsymbol{u}}{\partial t} + \boldsymbol{u} \cdot \boldsymbol{\nabla} \boldsymbol{u} = -\boldsymbol{\nabla} p + \boldsymbol{\nabla} \cdot \boldsymbol{\tau} \tag{3}$$

where p is the pressure, $\boldsymbol{\tau}$ is the stress tensor, and $\boldsymbol{u} = u\mathbf{e}_x + v\mathbf{e}_y + w\mathbf{e}_z$ is the velocity vector, in which u, v, w are the velocity components and $\mathbf{e}_x$, $\mathbf{e}_y$, $\mathbf{e}_z$ are the unite vectors in the streamwise, the cross-stream and the spanwise directions.

The constitutive equations for Herschel-Bulkley fluid are

$$\begin{cases} \boldsymbol{\tau} = \frac{1}{Re}\mu\dot{\boldsymbol{\gamma}} \Leftrightarrow \tau > \frac{B}{Re}, \\ \dot{\gamma} = 0 \Leftrightarrow \tau \leq \frac{B}{Re}, \end{cases} \tag{4}$$

where the effective viscosity is

$$\mu = \dot{\gamma}^{n-1} + \frac{B}{\dot{\gamma}}, \tag{5}$$

and $\dot{\gamma}$, τ are given by

$$\dot{\gamma} = [\frac{1}{2}\dot{\gamma}_{ij}\dot{\gamma}_{ij}]^{1/2}, \tau = [\frac{1}{2}\tau_{ij}\tau_{ij}]^{1/2}. \tag{6}$$

The Bingham number B and the Reynolds number Re are defined as

$$B = \frac{\tau_0 d}{\hat{\mu}_0 U_0}, \quad Re = \frac{\rho U_0 d}{\hat{\mu}_0}, \tag{7}$$

where $\hat{\mu}_0$ is defined as $K(U_0/d)^{n-1}$.

2.1. Linearized equations

Considering an infinitesimal disturbance $\boldsymbol{u}', p'$ to the base flow, $\boldsymbol{u}, p$ can be decomposed as $(\boldsymbol{u}, p) = (\bar{\boldsymbol{u}} + \boldsymbol{u}', \bar{p} + p')$. The base flow considered is a steady one driven by an imposed pressure gradient $-P_0$ in the x-direction, i.e.

$$p = -P_0 x. \tag{8}$$

The velocity of the base flow is one-dimensional and can be written in the form of $\bar{\boldsymbol{u}} = (U_b(y), 0, 0)$. The expression of the velocity profile $U_b(y)$ is

$$U_b(y) = \begin{cases} 1, & 0 \leq \mid y \mid < y^*, \\ 1 - (y - y^*)^{\frac{n+1}{n}}, & y^* \leq \mid y \mid \leq 1 + y^*, \end{cases} \tag{9}$$

where $y^* = l/d$ denotes the position of the yield surface. The Bingham number and the position of the yield surface have the relation of

$$B = (\frac{n+1}{n})^n y^*. \tag{10}$$

Subtracting the equations for the base and perturbed state, the linearized evolution equations for disturbance can be written as:

$$\boldsymbol{\nabla} \cdot \boldsymbol{u}' = 0, \tag{11}$$

$$\frac{\partial \boldsymbol{u}'}{\partial t} + \bar{\boldsymbol{u}} \cdot \boldsymbol{\nabla} \boldsymbol{u}' + \boldsymbol{u}' \cdot \boldsymbol{\nabla} \bar{\boldsymbol{u}} = -\boldsymbol{\nabla} p' + \boldsymbol{\nabla} \cdot \boldsymbol{\tau}', \tag{12}$$

where $\boldsymbol{\tau}'$ is the shear stress perturbation given by $\boldsymbol{\tau}' = (\bar{\mu}\dot{\boldsymbol{\gamma}}' + \mu'\bar{\dot{\boldsymbol{\gamma}}})/Re$.

The viscosity perturbation μ' can be express as

$$\mu' = \frac{\mathrm{d}\mu}{\mathrm{d}\dot{\gamma}} \mid_{\boldsymbol{u}=\bar{\boldsymbol{u}}} \dot{\gamma}' = \frac{\mathrm{d}\mu}{\mathrm{d}\dot{\gamma}} \mid_{\boldsymbol{u}=\bar{\boldsymbol{u}}} \mathtt{Sgn}(\bar{\gamma}_{xy})\gamma'_{xy}, \tag{13}$$

and $\mu'\bar{\dot{\boldsymbol{\gamma}}}$ is given by

$$\mu'\bar{\dot{\boldsymbol{\gamma}}} = \frac{\mathrm{d}\mu}{\mathrm{d}\dot{\gamma}} \mid_{\boldsymbol{u}=\bar{\boldsymbol{u}}} \bar{\dot{\gamma}}(\gamma'_{xy}\mathbf{e}_x \otimes \mathbf{e}_y + \gamma'_{yx}\mathbf{e}_y \otimes \mathbf{e}_x). \tag{14}$$

It can be shown straightforwardly that

$$\tau'_{ij} = \begin{cases} \frac{1}{Re}\bar{\mu}\dot{\gamma}'_{i,j} & for \quad ij \neq xy, yx \\ \frac{1}{Re}\mu_t\dot{\gamma}'_{i,j} & for \quad ij = xy, yx \end{cases} \tag{15}$$

where

$$\mu_t = \bar{\mu} + \frac{\mathrm{d}\mu}{\mathrm{d}\dot{\gamma}} \mid_{\boldsymbol{u}=\bar{\boldsymbol{u}}} \bar{\dot{\gamma}}, \tag{16}$$

in which μ_t is termed the *tangent viscosity*. For a non-Newtonian fluid, the different between μ_t and $\bar{\mu}$ identifies the departure from Newtonian viscosity. For a Herschel-Bulkley fluid, $\mu_t - \bar{\mu} = (n-1)\dot{\gamma}^{n-1} - B/\dot{\gamma}$.

As the flow is assumed periodic in the streamwise and the spanwise directions, all solutions to the linearized controlling equations can be expressed as superpositions of complex Fourier modes

$$[\boldsymbol{u}'(x,y,z,t), p'(x,y,z,t), h'(x,y,t)] = [\hat{\boldsymbol{u}}(y,t), \hat{p}(y,t), \hat{h}(t)]e^{i(\alpha x+\beta z)}, \tag{17}$$

in which the streamwise and the spanwise wavenumbers $\alpha, \beta \in \mathscr{R}$, h' is the perturbation of the yield surface.

At last the flowing initial value problem is obtained:

$$i\alpha\hat{u} + \mathtt{D}\hat{v} + i\beta\hat{w} = 0, \tag{18}$$

$$\frac{\partial\hat{u}}{\partial t} = -i\alpha\hat{p} - i\alpha U_b\hat{u} - \hat{v}\mathtt{D}\bar{u} + \frac{1}{Re}[\bar{\mu}(\mathtt{D}^2 - k^2)\hat{u} + \mathtt{D}\bar{\mu}_t(\mathtt{D}\hat{u} + i\alpha\hat{v}) + (\mu_t - \bar{\mu})(\mathtt{D}^2\hat{u} + i\alpha\mathtt{D}\hat{v})], \tag{19}$$

$$\frac{\partial\hat{v}}{\partial t} = -\mathtt{D}\hat{p} - i\alpha U_b\hat{v} + \frac{1}{Re}[\bar{\mu}(\mathtt{D}^2 - k^2)\hat{v} + 2\mathtt{D}\bar{\mu}\mathtt{D}\hat{v} + (\mu_t - \bar{\mu})i\alpha(\mathtt{D}\hat{u} + i\alpha\hat{v})], \tag{20}$$

$$\frac{\partial\hat{w}}{\partial t} = -i\beta\hat{p} - i\alpha U_b\hat{w} + \frac{1}{Re}[\bar{\mu}(\mathtt{D}^2 - k^2)\hat{w} + \mathtt{D}\bar{\mu}(\mathtt{D}\hat{w} + i\beta\hat{v})], \tag{21}$$

where $\mathtt{D}$ denotes $\frac{\mathtt{d}}{\mathtt{d}y}$.

The boundary conditions at the channel wall, $y = 1 + y^*$, are given by the no slip assumption and impermeability

$$\hat{u} = \hat{v} = \hat{w} = 0. \tag{22}$$

The boundary conditions at the unperterbed yield surface, $y = y^*$, are

$$\hat{u} = \hat{v} = \hat{w} = 0. \tag{23}$$

$$\mathtt{D}\hat{v} = \mathtt{D}\hat{w} = 0, \mathtt{D}\hat{u} = -\hat{h}\mathtt{D}^2\bar{u}. \tag{24}$$

The boundary conditions for a plane Bingham-Poiseuille flow has been derived by Nouar *et al.* [21]. The Dirichlet boundary conditions $\boldsymbol{u}' = 0$ at the yield surface come from the fact that the unyielded plug zone is constrained to move as a rigid body according to the Bingham model. With the help of velocity continuity across the yield surface, it follows that the fluid particles at the yield surface satisfy

$$\frac{\partial}{\partial x}\boldsymbol{u}' = \frac{\partial}{\partial z}\boldsymbol{u}' = 0 \tag{25}$$

The Neumann conditions come from linearization of the condition $\dot{\boldsymbol{\gamma}}(\bar{\boldsymbol{u}}+\boldsymbol{u}') = 0$, at the perturbed yield surface, onto the unperturbed yield surface position.

The controlling equations and the boundary conditions can be expressed in vector form

$$\mathscr{B}\frac{\partial}{\partial t}\boldsymbol{q} = \mathscr{A}\boldsymbol{q}, \tag{26}$$

in which $\boldsymbol{q} = (\hat{u}, \hat{v}, \hat{w}, \hat{p}, \hat{h})^T$. Finally, we obtain the linear initial value problem

$$\frac{\partial}{\partial t}\boldsymbol{q} = -i\mathscr{L}\boldsymbol{q}, \tag{27}$$

in which $\mathscr{L} = i\mathscr{B}^{-1}\mathscr{A}$.

3. Numerical method

In the present paper, we will study the nonmodal stability, i.e. the optimal disturbances in the form of initial conditions. Quest for maximum amplification of initial conditions is of particular interest in many hydrodynamic stability problems. For the linear system (27), the solution has the form

$$\boldsymbol{q}(t) = \exp(-i\mathscr{L}t)\boldsymbol{q}(0). \tag{28}$$

The maximum amplification of initial condition can be described by the growth function $G(t)$ as

$$G(t) = \max_{\boldsymbol{q}(0)\neq 0} \frac{\| \boldsymbol{q}(t) \|^2}{\| \boldsymbol{q}(0) \|^2} = \| e^{-i\mathscr{L}t} \|^2 . \tag{29}$$

We should note that $G(t)$ are related to the choice of definition of the norm $\|\cdot\|$. In the present paper, we choose the norm $\|\cdot\|$ as the energy norm. For variable $\boldsymbol{q}$, we will make use of a scalar product based on energy density defined as

$$(\boldsymbol{q}_1, \boldsymbol{q}_2)_{\mathscr{M}} = \int_{y^*}^{1+y^*} (\hat{u}_1 \hat{u}_2^* + \hat{v}_1 \hat{v}_2^* + \hat{w}_1 \hat{w}_2^*) \mathtt{d}y, \tag{30}$$

in which $*$ denotes the complex conjugate. Based on this scalar product, the associated energy norm is given as follows:

$$\|\boldsymbol{q}\|_{\mathscr{M}}^2 = (\boldsymbol{q}, \boldsymbol{q})_{\mathscr{M}} = \int_{y^*}^{1+y^*} (|\hat{u}|^2 + |\hat{v}|^2 + |\hat{w}|^2) \mathtt{d}y. \tag{31}$$

The spectral method can yield great accuracy for hydrodynamic stability problems. In the present paper, a Chebyshev-collocation method is used to solve the eigenvalue problem. We first transform the physical domain of $[y^*, 1+y^*]$ into the computational domain $[-1, 1]$ by introducing

$$\zeta = 2(y - y^*) - 1. \tag{32}$$

The variables $\hat{\boldsymbol{u}}$ and $\hat{p}$ are expanded as

$$\hat{\boldsymbol{u}} = \sum_{n=0}^{N} \hat{\boldsymbol{u}}_n T_n(\zeta), \hat{p} = \sum_{n=0}^{N} \hat{p}_n T_n(\zeta), \tag{33}$$

in which T_n denotes the n-th Chebyshev polynomial.

Using the Chebyshev series (33) and substituting $\partial/\partial t$ with $-i\omega$, the governing equations can be written in a discrete form as

$$\mathcal{A}\mathbf{x} = \omega \mathcal{B}\mathbf{x}, \tag{34}$$

in which $\mathbf{x}$ is the vector consisting of the spectral coefficients of $\hat{\boldsymbol{u}}$ and $\hat{p}$, and $\mathcal{A}, \mathcal{B}$ arise from discretization of the controlling equations and boundary conditions. This system of equations is required to solve for $4N + 5$ unknowns. The numerical method for general eigenvalue problem in the form $\mathcal{A}\mathbf{x} = \omega\mathcal{B}\mathbf{x}$ has been described by Canuto *et al.* [32].

For the present problem, it is notable that when direct solving the equation (18)-(24) the spectra (eigenvalues) do not converge due to the stiffness of the

problem. We observed that the viscosity dramatically becomes large near the point of inflection of the velocity. The reason for the non-convergence is that the power-law terms in the viscosity, including $\bar{\mu}$, μ_t and their derivatives, give rise to a highly stiff problem. In order to overcome the difficulty, it is essential to reduce the stiffness of the problem. In the controlling equations of the stability problem, near the point of inflection of the velocity the items related to $\bar{\mu}$, μ_t have very large values. One effective way to reduce the stiffness of problem is to divided the each equation by a factor F which is defined as $F = \max(\bar{\mu}, \mu_t, \mathtt{D}\bar{\mu}, \mathtt{D}\mu_t)$. For the energy stability problem in the subsequent section, this way is also need to reduce the stiffness of the eigenvalue problem.

The computation of the energy growth function $G(t)$ can be accomplished using an eigenvector expansion method in which eigenvectors are obtained from the Chebyshev-collocation method. For the procedure of this approach, we refer the reader to Ref.[16].

4. Results and discussions

For the present problem, the stability of a Fourier mode is determined by the parameters n, B, Re, α and β. We will investigate the energy stability and the nonmodal stability for the present problem.

4.1. condition for no energy growth

In this subsection, we are interested in the condition for which there is no growth of the perturbation kinetic energy. Energy methods give conditions for no energy growth. For hydrodynamics stability problems, the linear stability theory gives the sufficient conditions for instability, and the energy theory gives the sufficient conditions for stability. We now examine the condition below which the kinetic energy of an infinitesimal disturbance decays monotonically. Assuming the perturbation is periodic in the streamwise (x) and the spanwise (z) directions, the kinetic energy of perturbation confined to a single wavenumber can be defined in terms of the Fourier coefficients

$$E = \langle \hat{u}\hat{u}^* + \hat{v}\hat{v}^* + \hat{v}\hat{v}^* \rangle, \tag{35}$$

where $\langle\cdot\rangle$ denotes $\frac{\alpha\beta}{8\pi^2}\int_{y^*}^{y^*+1}\int_0^{2\pi/\alpha}\int_0^{2\pi/\beta}(.)\mathtt{d}z\mathtt{d}x\mathtt{d}y$. It can be shown that

$$\frac{\mathtt{d}E}{\mathtt{d}t} = \mathscr{P}(\boldsymbol{u},p) + \mathscr{I}(\boldsymbol{u}) + \frac{1}{Re}\{\mathscr{V}_1(\boldsymbol{u}) + \mathscr{V}_2(\boldsymbol{u}) + \mathscr{V}_3(\boldsymbol{u})\}, \tag{36}$$

where the items $\mathscr{P}(\boldsymbol{u},p)$,$\mathscr{I}(\boldsymbol{u})$, and $\mathscr{V}_1(\boldsymbol{u})$,$\mathscr{V}_2(\boldsymbol{u})$, $\mathscr{V}_3(\boldsymbol{u})$ are expressed as

$$\begin{aligned}\mathscr{P}(\boldsymbol{u},p) &= -i\alpha\langle\hat{p}\hat{u}^* - \hat{p}^*\hat{u}\rangle - \langle(\mathtt{D}\hat{p})\hat{v}^* + (\mathtt{D}\hat{p})^*\hat{v}\rangle - i\beta\langle\hat{p}\hat{w}^* - \hat{p}^*\hat{w}\rangle, \\ &= \langle\hat{p}^*[i\alpha\hat{u} + \mathtt{D}\hat{v} + i\beta\hat{w}]\rangle + \langle\hat{p}[i\alpha\hat{u} + \mathtt{D}\hat{v} + i\beta\hat{w}]^*\rangle, \quad (37)\\ \mathscr{I}(\boldsymbol{u}) &= -\langle\mathtt{D}\bar{u}(\hat{v}\hat{u}^* + \hat{v}^*\hat{u})\rangle, \quad (38)\\ \mathscr{V}_1(\boldsymbol{u}) &= [\bar{\mu}(\mathtt{D}^2 - k^2)\hat{u}]\hat{u}^* + [\mathtt{D}\bar{\mu}_t(\mathtt{D}\hat{u} + i\alpha\hat{v}) + (\mu_t - \bar{\mu})(\mathtt{D}^2\hat{u} + i\alpha\mathtt{D}\hat{v})]\hat{u}^* + conj, \quad (39)\\ \mathscr{V}_2(\boldsymbol{u}) &= [\bar{\mu}(\mathtt{D}^2 - k^2)\hat{v}]\hat{v}^* + [2\mathtt{D}\bar{\mu}\mathtt{D}\hat{v} + (\mu_t - \bar{\mu})i\alpha(\mathtt{D}\hat{u} + i\alpha\hat{v})]\hat{v}^* + conj, \quad (40)\\ \mathscr{V}_3(\boldsymbol{u}) &= [\bar{\mu}(\mathtt{D}^2 - k^2)\hat{w}]\hat{w}^* + [\mathtt{D}\bar{\mu}(\mathtt{D}\hat{w} + i\beta\hat{v})]\hat{w}^* + conj. \quad (41)\end{aligned}$$

There is no energy growth if the right-hand side of Eq.(36) is negative. The condition of no energy growth is given by the largest value of Re_1 such that

$$\frac{1}{Re_1} = \sup_{\boldsymbol{u}}\left\{-\frac{\mathscr{P}(\boldsymbol{u},p) + \mathscr{I}(\boldsymbol{u})}{\mathscr{V}_1(\boldsymbol{u}) + \mathscr{V}_2(\boldsymbol{u}) + \mathscr{V}_3(\boldsymbol{u})}\right\}, \tag{42}$$

where $\boldsymbol{u}$ is an admissible perturbation satisfying the continuity equation and the boundary conditions. This optimization problem can be solved using a variational method. The Euler equations corresponding to (42) lead to the eigenvalue problem as follows

$$i\alpha\hat{u} + \mathtt{D}\hat{v} + i\beta\hat{w} = 0, \tag{43}$$

$$\lambda(i\alpha\hat{p} + \hat{v}\mathtt{D}\bar{u}) = (2\mu_t\mathtt{D}^2 - 2k^2\bar{\mu} + 2\mathtt{D}\mu_t\mathtt{D})\hat{u} + [i\alpha\mathtt{D}(2\mu_t - \bar{\mu}) + 2i\alpha(\mu_t - \bar{\mu})\mathtt{D}]\hat{v}, \tag{44}$$

$$\lambda(\mathtt{D}\hat{p} + \hat{u}\mathtt{D}\bar{u}) = [-i\alpha\mathtt{D}\bar{\mu} + 2i\alpha(\mu_t - \bar{\mu})\mathtt{D}]\hat{u} + [2\bar{\mu}(\mathtt{D}^2 - k^2) + 2\mathtt{D}\bar{\mu}\mathtt{D} - 2\alpha^2(\mu_t - \bar{\mu}) - \mathtt{D}^2\bar{\mu}]\hat{v} - i\beta\mathtt{D}\bar{\mu}\hat{w}, \tag{45}$$

$$\lambda i\beta\hat{p} = i\beta\mathtt{D}\bar{\mu}\hat{v} + [2\bar{\mu}(\mathtt{D}^2 - k^2) + 2\mathtt{D}\bar{\mu}\mathtt{D}]\hat{w} \tag{46}$$

The boundary conditions at the channel walls, $y = \pm(1 + y^*)$, are

$$\hat{u} = \hat{v} = \hat{w} = 0. \tag{47}$$

The boundary conditions at the unperturbed yield surface, $y = \pm y^*$, are

$$\hat{u} = \hat{v} = \hat{w} = \mathtt{D}\hat{v} = \mathtt{D}\hat{w} = 0. \tag{48}$$

The function $Re_1(\alpha, \beta)$ corresponds the smallest positive eigenvalue λ of Eq.(43)-(46). Fig.2 displays the curves of the critical energy Reynolds number Re_1 versus the streamwise wavenumber α for streamwise disturbance ($\beta = 0$) with various Bingham numbers. In each figure in Fig.2, it is observed that the critical Reynolds number significantly decreases with the decrease of n at all wavenumbers. This result means that the effect of shear thinning is destabilizing for streamwise disturbances at various Bingham numbers.

Fig.3 plots the curves of the critical energy Reynolds number versus the wavenumber for spanwise disturbance ($\alpha = 0$). It is shown that at small β the critical Reynolds number is insensitive to n. At large wavenumbers, it is obvious that the critical Reynolds number decreases with the decrease of n. In Fig.3 for spanwise disturbance, the wavenumber corresponding to the lowest bound of Re_1 increases with the increase of shear thinning. However, in Fig.2 for streamwise disturbance, the wavenumber corresponding to the lowest bound of Re_1 is not sensitive to shear thinning.

In order to know the effect of shear thinning on the energy stability of disturbances with streamwise and spanwise variations, in Fig.4 we plot the contours of $Re_1(\alpha, \beta)$ in the $\alpha - \beta$ plane for $n = 0.2$, 0.8 and B=0.02, 0.2, 2 and 20, respectively. Comparing Fig4(a) with (b), (c) with (d), (e) with (f), (g) with (h) for each value of B shows that with the decrease of n the critical energy Reynolds number decreases. For small Bingham numbers of B=0.02 and 0.2, the most unstable mode is achieved by spanwise disturbance ($\alpha = 0$) for both weakly shear-thinning ($n = 0.8$) and strongly shear-thinning ($n = 0.2$) cases. In Fig.4(e) for B=2, as $n = 0.8$ the most unstable mode is achieved by spanwise disturbance. As $n = 0.2$, in Fig.4(f) the most unstable mode becomes an

oblique disturbance with $\alpha \approx 1.7$, $\beta \approx 3.5$. For B=20, the most unstable mode is an oblique wave with $\alpha \approx 1$, $\beta \approx 1$ for n=0.8. As n decreases to 0.2, the most unstable mode becomes a streamwise disturbance with $\alpha \approx 1$.

In Fig.5, the curves of the critical Reynolds number and critical wavenumbers versus the Bingham number are given for various n. As shown in Fig.5(a), at small B, Re_1 slightly increases with B. At large Bingham numbers, Re_1 increases with B at the order of $B^{1/2}$. At all Bingham numbers, with the increase of n the critical energy Reynolds number increases.

In Fig.5(b), for each value of n, there are two switch points B_1 and B_2. At small Bingham numbers of $B < B_1$, the critical spanwise wavenumber is insensitive to the change of B. With the increase of n, the spanwise wavenumber decreases. In this case, the most unstable mode is in the form of spanwise disturbance ($\alpha = 0$). At $B = B_1$, the most unstable mode switches from the spanwise disturbance to an oblique wave. As $B_1 < B < B_2$, with the increase of B, the critical spanwise wave decreases and the streamwise wavenumber increases. With the increase of n, the streamwise wavenumber decreases. As $B > B_2$, the critical spanwise wavenumber decreases to be zero and the most unstable modes becomes streamwise disturbances. With the increase of n, the two switch points B_1 and B_2 increase.

4.2. Transient behavior and non-modal stability

In this subsection, we are interested in the problem of the transient energy growth of initial conditions. The energy growth function $G(t)$ identifies the optimal growth of energy at time t. We can define the energy growth maximized over time as

$$G_{max} = G(t_{opt}) = \max G(t), \quad t \geq 0. \tag{49}$$

Before we present the results of the nonmodal stability of the problem, it is helpful to recall the mechanisms of the transient energy growth in plane channel flows. It has been shown that, for inviscid shear flows, the streamwise velocity grows linearly with time for disturbance without streamwise variation

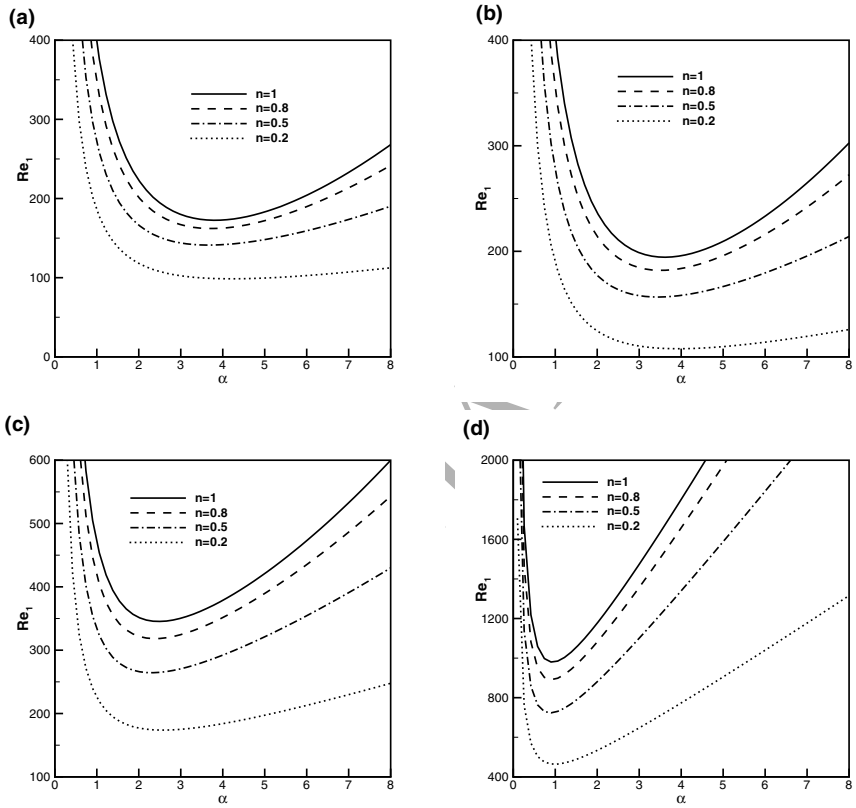

Figure 2: The curves of the critical energy Reynolds number Re_1 versus the streamwise wavenumber α for streamwise disturbances ($\beta = 0$). (a) $B = 0.02$, (b) $B = 0.2$, (c) $B = 2$, (d) $B = 20$.

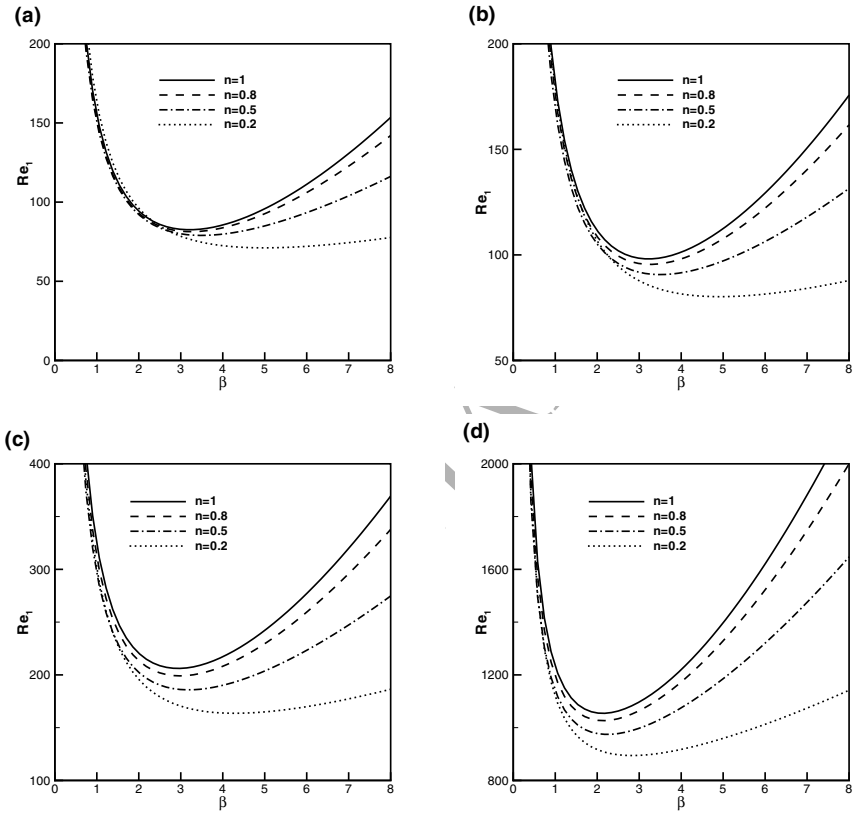

Figure 3: The curves of the critical energy Reynolds number Re_1 versus the spanwise wavenumber β for spanwise disturbances ($\alpha = 0$). (a) $B = 0.02$, (b) $B = 0.2$, (c) $B = 2$, (d) $B = 20$.

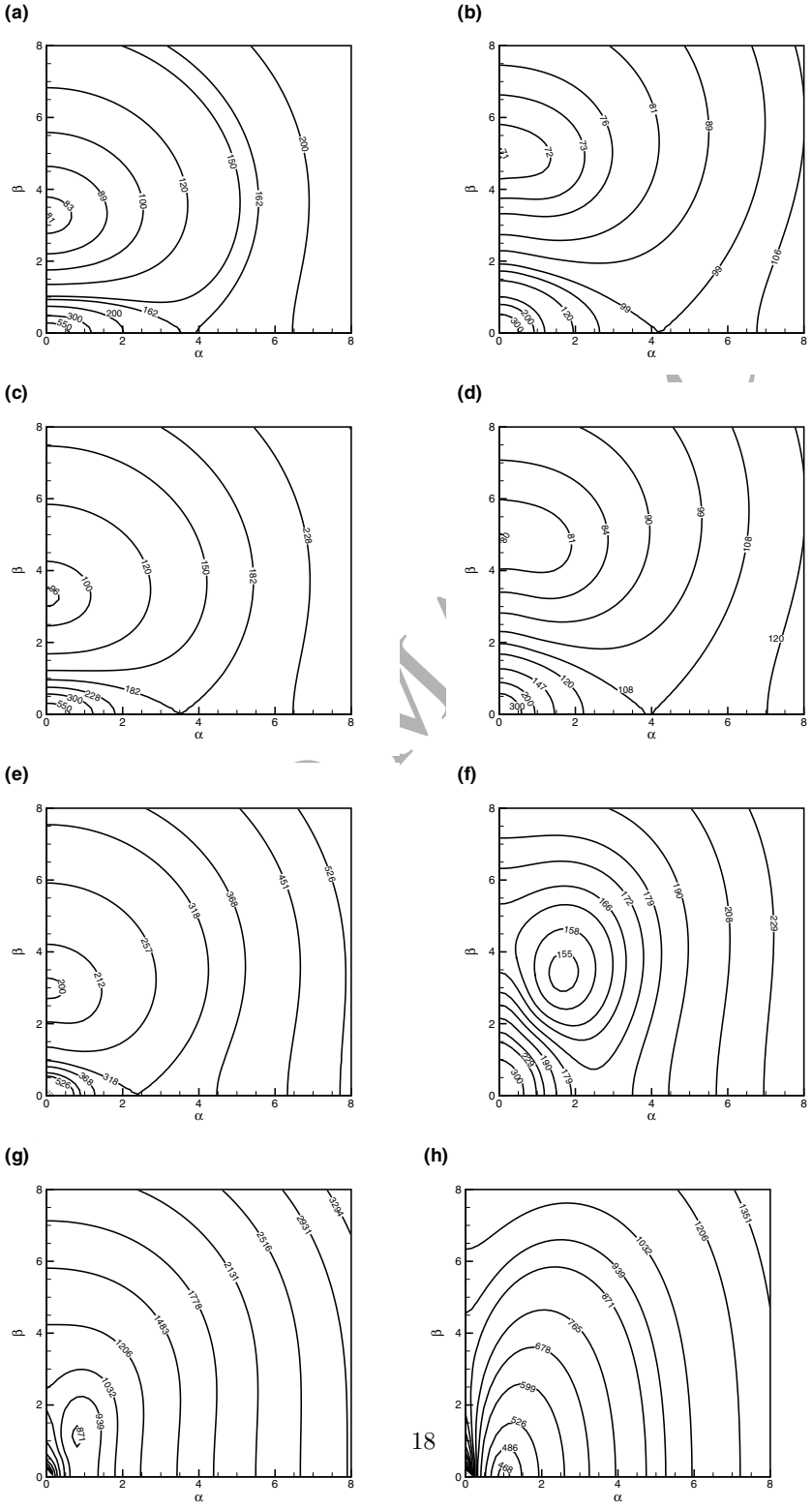

Figure 4: Contours of the critical energy Reynolds number Re_1 in the $\alpha - \beta$ plane. The Bingham numbers for (a)(b) , (c)(d), (e)(f) and (g)(h) are $B = 0.02$, 0.2, 2 and 20, respectively. The shear-thinning index is $n = 0.8$ for (a), (c), (e), (g) , and $n = 0.2$ for (b), (d), (f), (h).

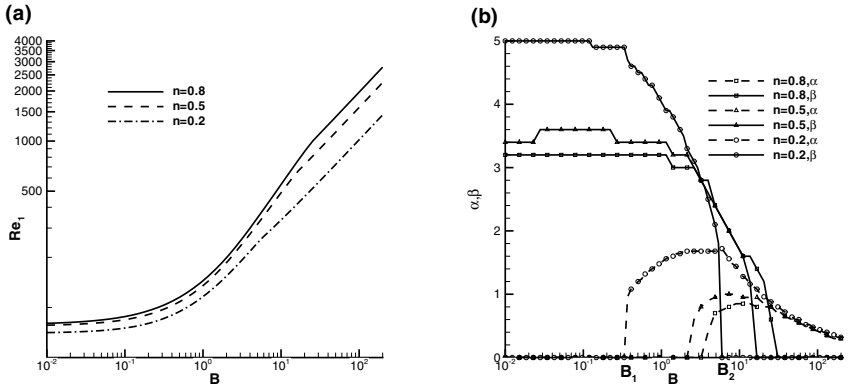

Figure 5: (a) The curves of the critical energy Reynolds number versus the Bingham number. (b) The curves of the critical streamwise wavenumber α and the spanwise wavenumber β of the most unstable modes versus the Bingham number.

$B = 0.02$:									
n	1	0.9	0.8	0.7	0.6	0.5	0.4	0.3	0.2
G_{max}	640.0	642.3	642.5	642.3	639.3	633.3	626.5	624.1	632.5
T_{opt}	95.0	92.2	89.2	72.9	70.2	66.3	50.7	45.9	34.2
$B = 2$:									
n	1	0.9	0.8	0.7	0.6	0.5	0.4	0.3	0.2
G_{max}	90.8	96.2	98.0	99.7	101.4	102.6	103.5	104.1	110.4
T_{opt}	30.0	23.5	23.3	21.6	21.1	19.2	18.4	15.4	11.0
$B = 20$:									
n	1	0.9	0.8	0.7	0.6	0.5	0.4	0.3	0.2
G_{max}	5.3	5.6	5.9	6.2	6.7	7.2	8.0	9.5	11.7
T_{opt}	9.4	9.6	9.9	10.0	9.8	10.0	9.5	9.3	9.0

Table 1: The energy growth of the optimal disturbance, G_{max}, and the optimal time t_{opt} for various B and n.

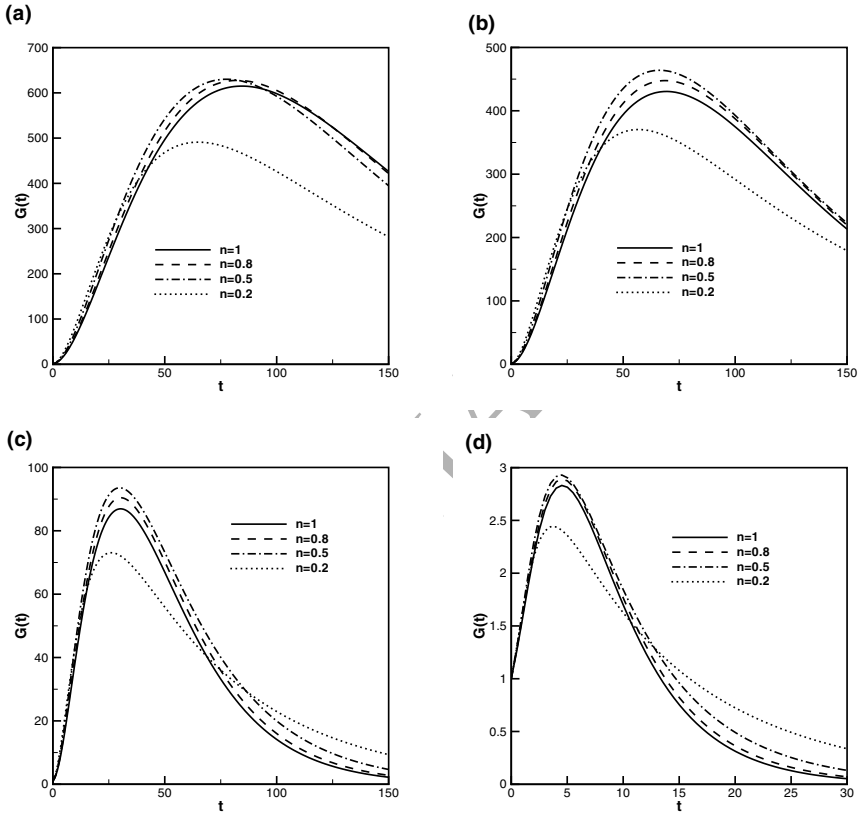

Figure 6: Energy amplifications for spanwise disturbances with $\beta = 4$ for various n at $Re = 3000$. (a) $B = 0.02$; (b) $B = 0.2$; (c) $B = 2$; (d) $B = 20$.

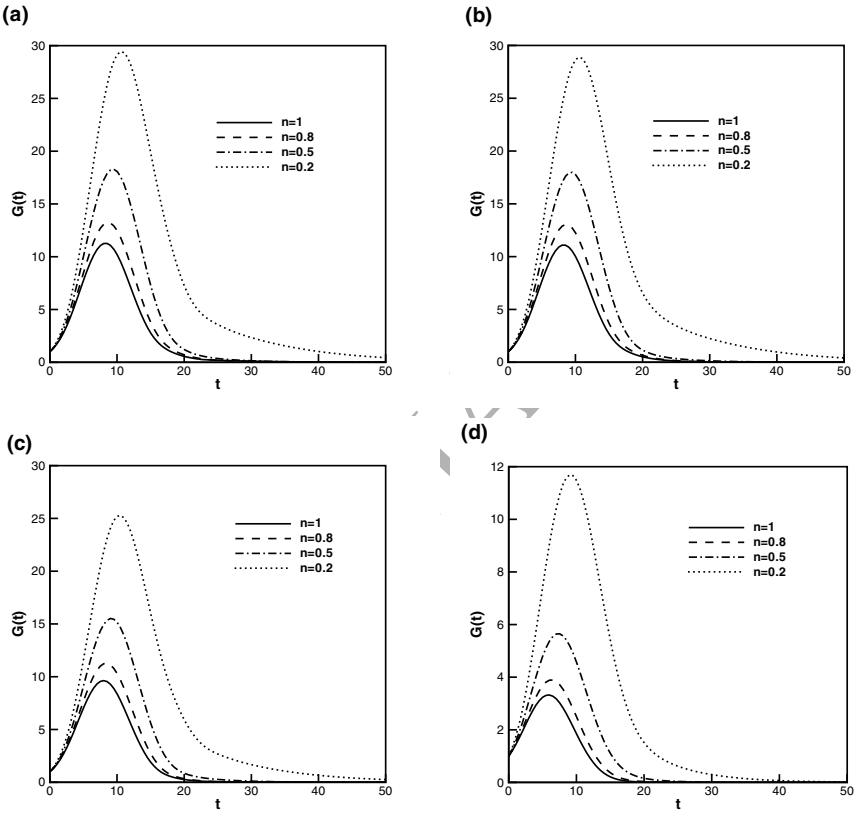

Figure 7: Energy amplification for streamwise disturbance with $\alpha = 2$ for various n at $Re = 3000$. (a) $B = 0.02$; (b) $B = 0.2$; (c) $B = 2$; (d) $B = 20$.

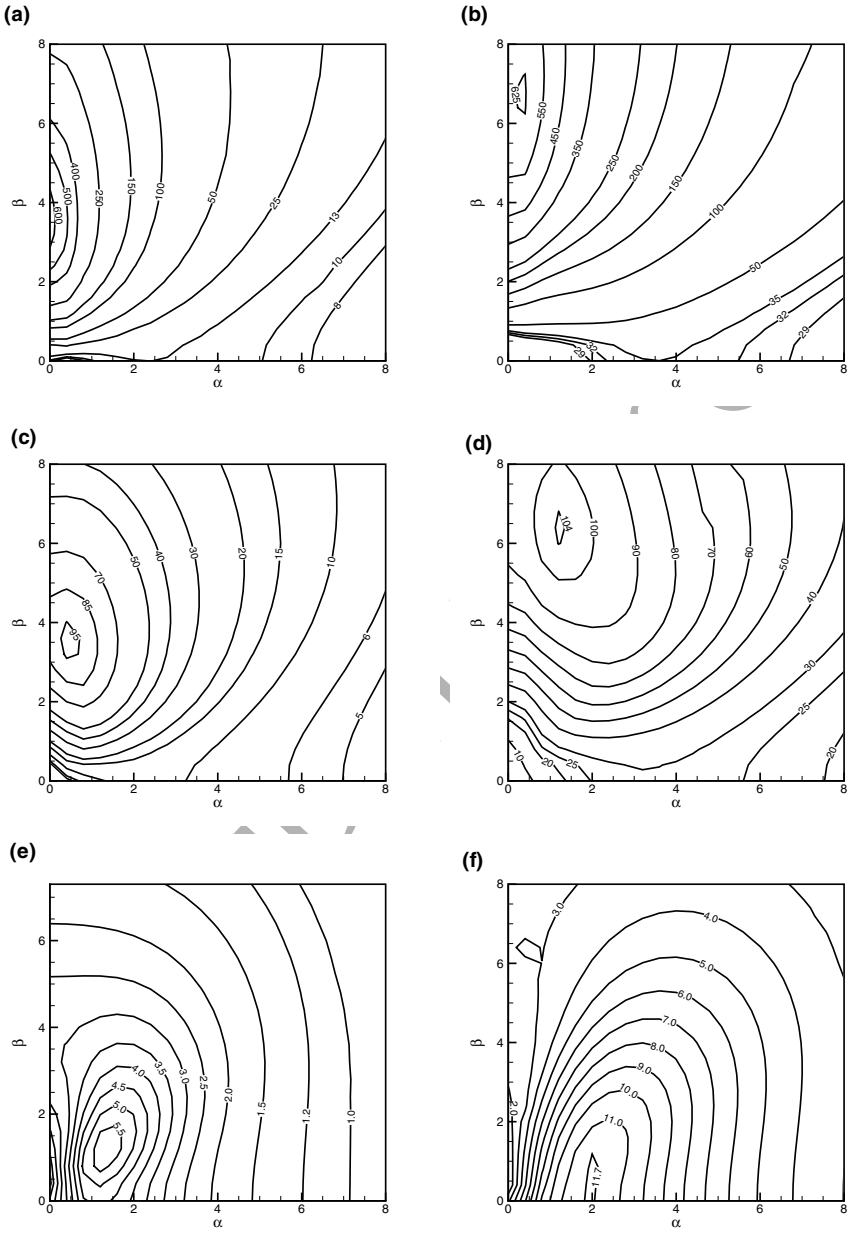

Figure 8: Contours of the maximum energy growth rate G_{max} in the $\alpha-\beta$ plane at $Re = 3000$. (a) $B = 0.02$, $n = 0.8$; (b) $B = 0.02$, $n = 0.2$; (c) $B = 2$, $n = 0.8$; (d) $B = 2$, $n = 0.2$; (e) $B = 20$, $n = 0.8$; (f) $B = 20$, $n = 0.2$.

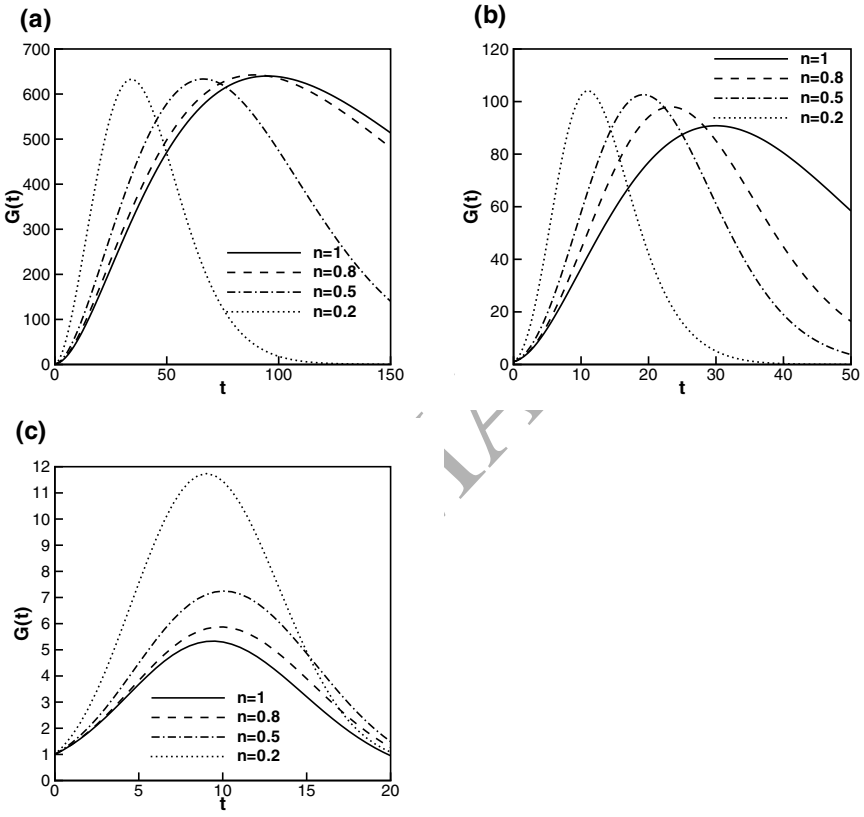

Figure 9: Energy amplifications of the optimal disturbances with various shear-thinning index n. (a) $B = 0.02$; (b) $B = 2$; (d) $B = 20$.

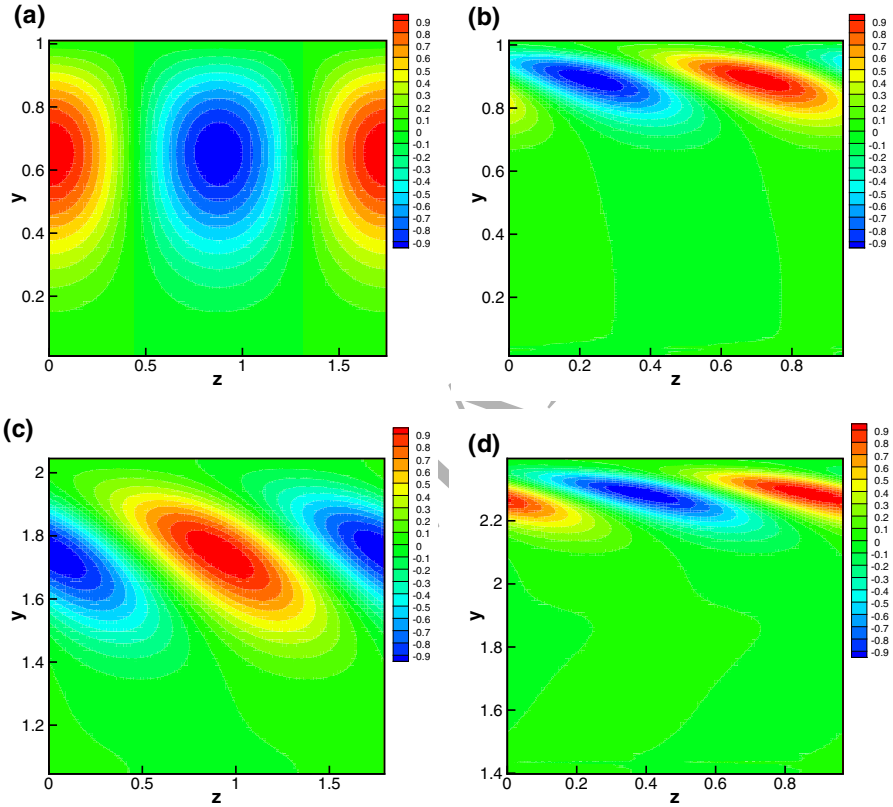

Figure 10: Cross-stream ($y-z$) view of the streaky structure of the optimal flow at $Re = 3000$. The contours denote the values of streamwise velocity u. (a) $B = 0.02$, $n = 0.8$; (b) $B = 0.02$, $n = 0.2$; (c) $B = 2$, $n = 0.8$; (d) $B = 2$, $n = 0.2$.

[37]. This growth mechanism has been labelled 'lift-up' and vortex stretching, or more accurately vortex tilting [15]. For viscous shear flows the streamwise velocity grows linearly with time due to the lift-up mechanism before being damped by the viscosity [19]. In addition to the lift-up effect, another growth mechanism, i.e. two-dimensional Reynolds stress mechanism [35] is responsible to the energy growth of spanwise uniform disturbances.

For the present problem, if the Reynolds number is less than the critical energy Reynolds number Re_1, then $G(t) \leq 1$ for all time. In this case, $G_{max} = 1$ and $t_{opt} = 0$. If the Reynolds number exceeds the critical Reynolds number Re_2 such that the linear operator has an unstable eigenvalue, then $G_{max} \to \infty$ at $t_{opt} \to \infty$. If $Re_1 < Re < Re_2$, the flow is linearly stable but has a transient energy growth. For general stability problems, these three types of behaviors should be considered. However, for the present problem, we have not found unstable eigenvalues for a wide range of Reynolds numbers. So, when examining the nonmodal stability, we only consider the case of $Re > Re_1$.

In order to know the effect of shear thinning at various Bingham numbers, we plot, in Fig.6 and Fig.7, the curves of the energy growth function $G(t)$ with various index n for different Bingham numbers. As shown in Fig.6 for spanwise disturbances, each curve experiences an energy growth and then gradually decreases with time. For B=0.02, 0.2 and 2, the energy growth is much larger than that of the large Bingham number of B=20. In each figure, for weakly shear-thinning fluids of $n \geq 0.5$, with the decrease of n the energy growth rate slightly increases. As n decreases to 0.2, the energy growth decreases significantly. It seems that for spanwise disturbances, the maximum energy growth G_{max} does not monotonously increase or decrease with n.

In Fig.7, we plot the curves of the transient energy growth for streamwise disturbances. In these figures for different B, with the increase of shear thinning the transient energy growth $G(t)$ increases.

In Fig.6 and 7, we have examined the transient energy growth of the spanwise and streamwise disturbances. In order to know the energy growth of oblique disturbances, we examine the maximal energy growth G_{max} in the α-β plane.

In Fig.8, the isolines of G_{max} are plotted for various B and n at $Re = 3000$. Comparing Fig.8(a) with (b), (c) with (d) and (e) with (f), we found that with the decrease of n the optimal energy growth increases. In Fig.8(a), for B=0.02 and n=0.8 the optimal disturbance is realized at $\alpha \approx 0$ and $\beta \approx 3.5$. The optimal disturbance is in the form of streamwise independent vortices and streaks. As n decreases to 0.2, in Fig.8(b) the optimal disturbance is realized at $\alpha \approx 0.3$ and $\beta \approx 6.7$. In Fig.8(c) for B=2 and n=0.8, the optimal disturbance is a weakly oblique wave, i.e. the streamwise wavenumber is much smaller than the spanwise wavenumber. As n decreases to 0.2, in Fig.8(d) both the streamwise and the spanwise wavenumbers of the optimal disturbance increases. For large Bingham number $B = 20$, at $n = 0.8$ the optimal disturbance is an oblique wave. As n decreases to 0.2 the optimal mode is in the form of streamwise disturbance.

Fig.9, we plot the curves of the energy growth for the optimal disturbances for various B with different streamwise and spanwise wavenumbers. In Table 1, we present the values of the maximum energy growth G_{max} and the optimal time t_{opt} for more values of n and different Bingham numbers. As shown in Fig.9(a) for small Bingham number, $B = 0.02$, the difference between the maximum values of $G(t)$ of these curves are slight. Both the curves in Fig.9(a) and the value of G_{max} listed in Table 1 show that G_{max} is insensitive to the shear-thinning index n and the shear thinning only influences the optimal time t_{opt}. As shown in Fig.9(b) and Table 1 for medium Bingham number, $B = 2$, G_{max} increases with the increase of shear thinning. For these two cases, it is obvious that the time t_{opt} at which the maximum growth occurs decreases with the increase of shear thinning. For large Bingham number, $B = 20$, as shown in Fig.9(c) and Table 1, the maximum energy growth is much lower that in Fig.9(a) and (b). In Fig.9(c), the maximum energy growth G_{max} increases with the shear thinning, but the optimal time t_{opt} is insensitive to n.

It is interesting to compare the influence of n on the transient energy growth of the present problem with that of the plane Poiseuille flow of a shear-thinning fluid without an unyielded zone. Nouar *et al.* [28] have shown that for the

plane Poiseuille flow of a shear-thinning fluid the shear thinning is to reduce significantly the maximum growth by the approximate scalings of $G_{max} \sim n^{3.60}$. However, for the present problem no scaling law between n and G_{max} exists for various B.

As shown in Fig.8, for small or medium Bingham numbers, the streamwise wavenumbers of the optimal disturbances are much smaller than the spanwise wavenumbers. At the optimal time t_{opt}, the optimal disturbances are close to streaks. In order to know the effect of shear thinning on the streaky structure of disturbance with optimal energy growth, we plot in Fig.10 the flow fields of the optimal disturbance at the optimal time t_{opt}. For small Bingham number of $B = 0.02$ and weakly shear-thinning fluid of $n = 0.8$, as shown in Fig.10(a) the flow fields is characterized by two straight streaks. The streaky structure in Fig.10(a) is very similar to that of a plane Poiseuille flow of a Newtonian fluid [16] in which the lift-up mechanism is responsible for the energy growth. In Fig.10(b) for strongly shear-thinning fluid of $n = 0.2$, the centers of the streaks shift towards the wall region. Moreover, the streaks become oblique and a stagnant region appears near the yield surface. For medium Bingham number of $B = 2$, as shown in Fig.10(c) and (d) for $n = 0.8$ and 0.2, the optimal disturbances are in the form of oblique streaks. Being similar to that in Fig.10(a) and (b) for $B = 0.02$, with the increase of shear thinning, the centers of the streaks shift towards the wall region.

It is well known that the lift-up and the Orr mechanisms are responsible for 2D and 3D optimal energy growth of disturbances, respectively [16, 19]. For the optimal disturbances in the form of oblique waves, both mechanisms play roles in the amplification of the energy. However, it is difficult to compare the contributions of the lift-up and the Orr mechanisms to the energy amplification of the optimal disturbance as they act simultaneously. Vitoshkin *et al.* [38] examined the mechanism of the three-dimensional optimal energy growth, in plane parallel shear flows, in terms of the role of vortex stretching and the interplay between the spanwise vorticity (q) and the planar divergent components (d). The authors expected that optimal growth occurs when the interplay between

d and q results in a simultaneous growth of the two fields.

In order to evaluate the contributions of the lift-up and the Orr mechanisms, we plot in Fig.11 the evolution of energy of the optimal disturbances for various parameters. As shown in Fig.11(a) and 11(b) for $B = 0.02$, the streamwise wavenumber α is much smaller than the spanwise wavenumber β, the curves of E and E_v almost coincide. This indicates that the streaks occupy most of kinetic energy of the disturbance. In Fig.11(c) and 11(d) for $B = 2$, the curve of E_v is slightly lower than that of E. From Fig.11(a) to 11(d), we can expected that for streamwise uniform streaks or weakly oblique streaks, the life-up mechanism is responsible for most of the energy growth. In Fig.11(e) and 11(f) for large Bingham number of $B = 20$, the optimal disturbance is in the form of strongly oblique wave. In these two figures, the energy of the streaks is obviously smaller than that of the total energy growth of the disturbance. In this case, the contributions of the lift-up mechanism and the Orr mechanism are comparable.

5. Conclusions

In the present paper, the linear stability in plan Poiseuille flow of a Herschel-Bulkley fluid is studied using the energy method and the nonmodal stability theory. The base flow is characterized by an unyielded zone moving with a constant velocity and shear thinning of the viscosity between the channel wall and the yield surface. The problem are controlled by three dimensionless parameters: the shear-thinning index n, the Bingham number B and the Reynolds number Re. For the base flow, the position of the yield surface is determined by both B and n. We focus on the effect of shear thinning on the stability of the flow.

The results of energy stability shows that the relation between the critical energy Reynolds number and the Bingham number is similar for both the strongly and weakly shear-thinning fluids. For small B, Re_1 is insensitive to B and slightly increases with the increase of B. However, for large B, Re_1

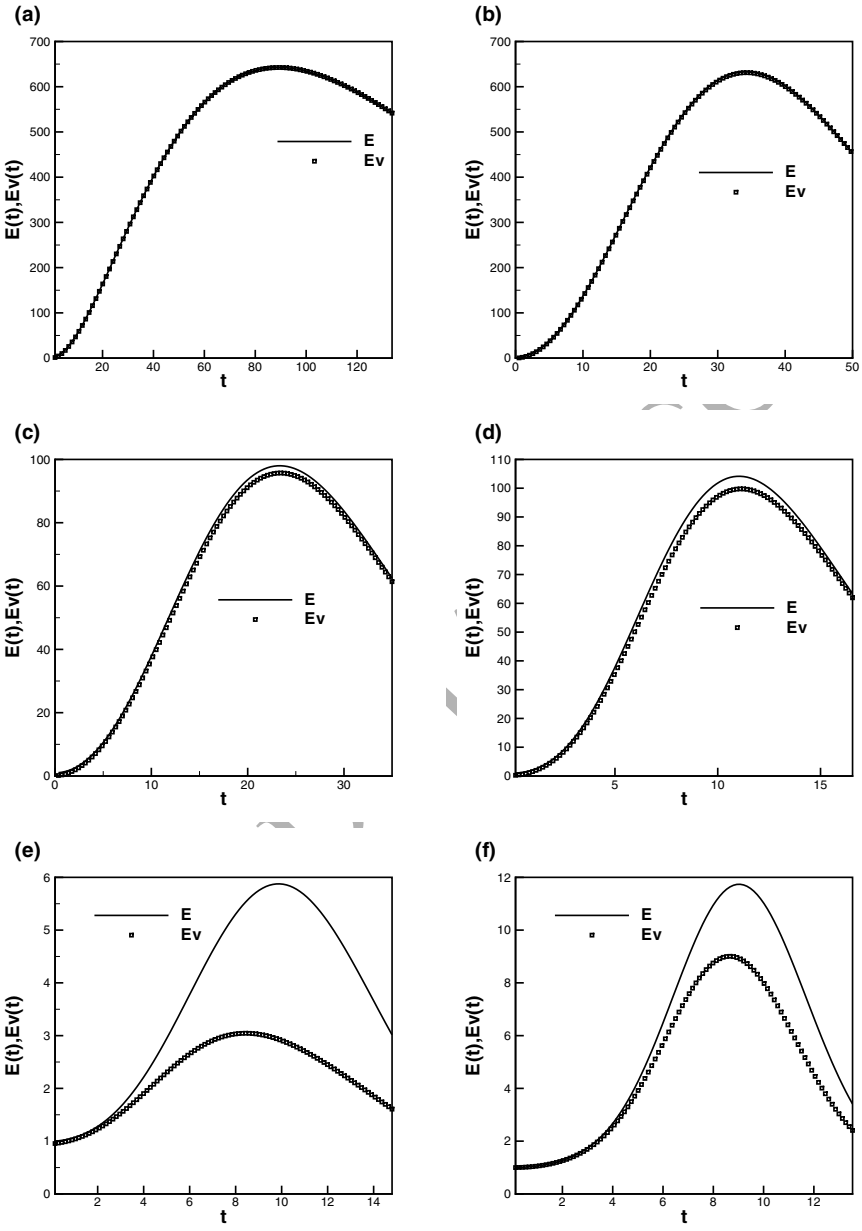

Figure 11: The evolution of the energy of the optimal perturbation over time. E denotes the total energy of the disturbance. E_v denotes the energy of the streak. Other parameters are (a) $B = 0.02$, $n = 0.8$, $\alpha = 0$, $\beta = 3.6$; (b) $B = 0.02$, $n = 0.2$, $\alpha = 0.3$, $\beta = 6.65$; (c) $B = 2$, $n = 0.8$, $\alpha = 0.5$, $\beta = 3.5$; (d) $B = 2$, $n = 0.2$, $\alpha = 1.4$, $\beta = 6.5$; (e) $B = 20$, $n = 0.8$, $\alpha = 1.3$, $\beta = 1.1$; (f) $B = 20$, $n = 0.2$, $\alpha = 2.0$, $\beta = 0.7$.

increases with B at the order of $B^{1/2}$.

The results of nonmodal stability analysis show that the parameter n and B play important roles in determining the energy growth and the structure of the optimal disturbance. With the increase of B the optimal energy growth decreases for both weakly and strongly shear-thinning fluids. At various value of B, the shear thinning plays different roles in influencing the optimal transient energy growth. At a very low Bingham number, the optimal disturbance is very close to spanwise disturbance for both weakly and strongly shear-thinning fluids. The maximum energy growth of the optimal disturbance is insensitive to the shear thinning. At a medium Bingham number, the optimal disturbance is an oblique wave. Both the streamwise and the spanwise wavenumbers increase with the increase of shear thinning. The maximum energy growth of the optimal disturbance increases with shear thinning. For low and medium Bingham numbers, with the increase of shear thinning, the centers of the streaky structures move towards the outer wall. At a high Bingham number, with the increase of shear thinning the optimal disturbance changes from an oblique wave into a streamwise disturbance.

Acknowledgments

This work was supported by National Natural Science Foundation of China (Grant Nos. 51766002, 11102211 and 11402271).

References

[1] R. Byron-Bird, G. C. Dai, and B. J. Yarusso, The rheology and flow of viscoplastic materials, Rev. Chem. Eng. 1 (1983) 1–70.

[2] R. P. Chhabra and J. F. Richardson, Non-Newtonian Flow and Applied Rheology: Engineering Applications, 2nd ed., Elsevier, 2008.

[3] R. B. Bird, R. C. Armstrong and O. Hassager, Dynamics of Polymeric Liquid, Vol I: Fluid Mechanics, John Wily & Sons Inc., 1977.

[4] R. B. Bird, W. E. Stewart and E. N. Lightfoot, Transport Phenomena, John Wily & Sons Inc., 2002.

[5] J. G. Oldroyd, Two-dimensional plastic flow of a Bingham solid, Proc. Camb. Phil. Soc. 43 (1947) 383–395.

[6] X. Huang and M. H. García, A Herschel-Bulkley model for mud flow down a slope, J. Fluid Mech. 374 (1998) 305–333.

[7] Q. D. Nguyen and D. V. Boger, Yield stress measurement for concentrated suspensions, J. Rheol. 27 (1983) 321–349.

[8] P. Coussot and J. M. Piau, On the behavior of fine mud suspensions, Rheol. Acta. 33 (1994) 175–184.

[9] S. A. Orszag, Accurate solution of the Orr-Sommerfeld equation, J. Fluid Mech. 50 (1971) 689–703.

[10] V. A. Romanov, Stability of plane-parallel Couette flow, Funct. Anal. Appl. 7 (1973) 137–146.

[11] V. C. Patel and M. R. Head, Some observation on skin friction and velocity profiles in fully developed pipe and channel flow, J. Fluid Mech. 38 (1969) 181–201.

[12] N. Tillmark and H. Alfredsson, Experiments on transition in plane Couette flow, J. Fluid Mech. 235 (1992) 89–102.

[13] P. J. Schmid, Nonmodal stability theory, Annu. Rev. Fluid Mech. 39 (2007) 129–162.

[14] F. Waleffe, On a self-sustaining process in shear flows, Phys. Fluids 9(4) (1997) 883-900.

[15] L. N. Trefethen, A. E. Trefethen, S. C. Reddy and T. A. Driscoll, Hydrodynamics stability without eigenvalues, Science 261 (1993) 578–584.

[16] S. Reddy and D. S. Henningson, Energy growth in viscous channel flows, J. Fluid Mech. 252 (1993) 209–238.

[17] M. T. Landahl, Wave breakdown and turbulence, SIAM J. Appl. Maths. 28 (1975) 735–756.

[18] M. T. Landahl, A note on an algebraic instability of inviscid parallel shear flows, J. Fluid Mech. 98 (1980) 243–251.

[19] B. F. Farrel and P. J. Ioannou, Optimal excitation of three-dimensiogal perturbations in viscous constant shear flow, Phys. Fluids A 6 (1993) 1390–1400.

[20] I. A. Frigaard, S. D. Howison and I. J. Sobey, On the stability of Poiseuille flow of a Bingham fluid, J. Fluid Mech. 263 (1994) 133–150.

[21] C. Nouar, N. Kabouya, J. Dusek and M. Mamou, Modal and non-modal linear stability of the plane Bingham-Poiseuille flow, J. Fluid Mech. 577 (2007) 211–239.

[22] C. Nouar and I. A. Frigaard, Nonlinear stability of Poiseuille flow of Bingham fluids: theoretical results and comparison with phenomenogical criteria, J. Non-Newtonian Fluid Mech. 100 (2001) 127–149.

[23] I. A. Frigaard and C. Nouar, On three-dimensional linear stability of Poiseuille flow of Bingham fluids, Phys. Fluids 15 (2003) 2843–2851.

[24] C. Nouar, N. Kabouya, J. Dusek and M. Mamou, Modal and non-modal linear stability of the plane Bingham-Poiseuille flow, J. Fluid Mech. 577 (2007) 211–239.

[25] A. Esmael and C. Nouar, Transitional flow of a yield-stress fluid in a pipe: Evidence of a robust coherent structure, Phys. Rev. E 77 (2008) 057302(1-4).

[26] R. Liu and Q. S. Liu, Non-modal stability in Hagen-Poiseuille flow of a Bingham fluid, Phys. Fluids 26 (2014) 014012(1–23).

[27] V. Chikkadi, A. Sameen and R. Govindarajan, Preventing transition to turbulence: a viscosity stratification does not always help, Phy. Rev. Lett. 95 (2005) 264504(1-4).

[28] C. Nouar, A. Bottaro and J. P. Brancher, Delaying transition to turbulence in channel flow: revisiting the stability of shear-thinning fluids, J. Fluid Mech. 592 (2007) 177–194.

[29] R. Liu and Q. S. Liu, Nonmodal stability in plane Couette flow of a power-law fluid, J. Fluid Mech. 676 (2011) 145–171.

[30] R. Liu and Q. S. Liu, Nonmodal stability in Hagen-Poiseuille flow of a shear thinning fluid, Phys. Rev. E 85 (2012) 066318(1–16).

[31] H. Bentrad, A. Esmael, C. Nouar, A. Lefevre and N. Ait-Messaoudene, Energy growth in Hagen-Poiseuille flow of Herschel-Bulkley fluid, J. Non-Newtonian Fluid Mech. 241 (2017) 43–59.

[32] C. Canuto, M. Y. Hussaini, A. Quarteroni and T. A. Zang, Spectral Method in Fluid Dynamics, Springer, 1993.

[33] B. Güzel, T. Burghelea, I. A. Frigaard and D. M. Martinez, Observation of laminar-turbulent transition of a yield stress fluid in Hagen-Poiseuille flow, J. Fluid Mech. 627 (2009) 97–128.

[34] L. N. Trefethen and M. Embree, Spectra and Pseudospectra: The Behavior of Nonnormal Matrices and Operators, Princeton University Press, 2005.

[35] J. Pedlosky, ,Geophysical Fluid Dynamics, 2nd ed., Springer, 1987.

[36] P. J. Schmid and D. S. Henningson, Stability and Transition in Shear Flows, Springer-Verlag New York Inc., 2001.

[37] T. Ellingsen and E. Palm, Stability of linear flow, Phys. Fluids 18 (1975) 487–488.

[38] H. Vitoshkin, E. Heifetz, A. Yu. Gelfgat and N. Harnik, On the role of vortex stretching in energy optimal growth of three-dimensional perturbations on plane parallel shear flows, J. Fluid Mech. 707 (2012) 369–380.